Available online at www.sciencedirect.com
ScienceDirect
Journal of the European Ceramic Society 30 (2010) 2057–2064
www.elsevier.com/locate/jeurceramsoc

Peculiarities of crystallization of alumina, yttria and rare-earth element oxides of yttria subgroup in an optical furnace

A.A. Frolov *, E.V. Voynich, V.V. Garbuz

I.N. Frantsevich Institute for Problems of Materials Science, NAS of Ukraine, 3 Krzhizhanovsky St., Kiev 03142, Ukraine

Received 5 June 2009; received in revised form 9 March 2010; accepted 2 April 2010

Abstract

The peculiarities crystallization of alumina, yttria and the rare-earth element oxides of the yttria subgroup in an optical furnace have been studied. Direct evidence of oxygen dissolution during alumina melting in oxidizing atmosphere and its ejection during crystallization has been presented. The released oxygen was captured by the inside hollows of alumina ingots, and its quantity was controlled using gas chromatography. It was not less than 8×10^{-6} g in 1 g of alumina. The quantity of the oxygen released is corresponding to that for REE oxides. The yttria specific volume increasing during crystallization was confirmed. The apparent ingot volume of Er, Ho, Tm, and Yb oxides does not change, while the specific volume of lutecia decreases.

Keywords: Crystallization; Thermal expansion; Al_2O_3; Y_2O_3; Refractories

1. Introduction

Alumina, rare-earth elements (REE) oxides and their alloys are used as refractories, ionic conductors, laser materials, etc. Alumina is the most researched material among them. To obtain high temperature oxides and their alloys, melting and crystallization of initial materials are widely used. That is why many researchers have investigated the density and surface tension of liquid Al_2O_3.[1–14] The melt density of yttrium and rare-earth oxides has been investigated by the levitation methods.[10,15] The influence of gas medium on melting and crystallization processes has been described.[13,16–21] Some authors did not observe any influence of the gas composition on the density of small alumina drops (<100 mg).[13] In some works the effect of gas medium on the alumina surface tension did not exceed the measurement error,[21] whereas in others the influence of gas composition on the properties of liquid and crystallized alumina had been found.[16–20] It has been shown that melting temperature of alumina is changing with the composition of gas medium (vacuum, air, argon or helium) by up to 6 °C.[16] The reflection power of melted alumina depends on the composition of gas medium (vacuum or air).[17,20] The ingots obtained in an oxidizing medium were white, while those obtained in argon (argon or vacuum) were grey. Nucleation in alumina melt depends on the oxygen partial pressure.[18] Overcooling of alumina melt as has been shown is depending on the gas medium (argon or oxygen).[19] The composition of the gas medium also influences the melting temperature of other oxides, for example TiO_2 and CoO.[22] The reason for the influence is deviation from the stoichiometry. It has been revealed, that the oxygen content in TiO_2 decreases upon melting in argon, whereas that in CoO increases in an oxidizing medium.[22] Experimental investigations and mathematical calculation of bubble forming in ruby crystals have been done in the work.[23–25] The author[23,24] has shown that if alumina (ruby) crystals are grown in argon atmosphere, the concentration of gas bubbles would be decrease greatly. Using nitrogen atmosphere gas bubbles concentration has been diminished, too. So, the author has made the conclusion if the alumina melting in air, the last is being solved in the melt. At alumina solidification the solved air is rejected from the melt. Herewith, gas bubbles are formed close to melt–solid interface and caught by the growing crystal. The author also proposed the calculation model of gas bubbles concentration. The author has made the conclusion that at the following conditions: slow growing rate, small crystal diameter, and used argon atmosphere, the crystals without bubbles can be obtained.[23,24] The authors[25] have been concluded,

* Corresponding author. Tel.: +380 44 393 0974; fax: +380 44 424 2131.
E-mail address: Al-frolov@yandex.ru (A.A. Frolov).

0955-2219/$ – see front matter © 2010 Elsevier Ltd. All rights reserved.
doi:10.1016/j.jeurceramsoc.2010.04.002

that the use of non-oxidant atmospheres is determinant in order to obtain Al_2O_3–$Y_3Al_5O_{12}$ and Al_2O_3–$Y_3Al_5O_{12}$–ZrO_2 eutectics with no porosity. This fact can be explained if oxygen is the gas dissolved in the melt.

Slight influence of oxygen medium on the melting temperature of REE oxides has been established as well.[26] So, it is reasonable to relate all these peculiarities of melting and crystallization of these oxides to deviation of the oxygen content from stoichiometry caused by different media.

Hence, oxygen and water vapor dissolution in melts of oxides should be taken into account. Here the release of oxygen and water vapor occurs upon crystallization, which is accompanied by intense gas bubble formation and melt splashing.[27–29] Dissolution of large quantity of oxygen was found in melts of complex alumina compounds with transition metals (Fe, Co, Ni, and Ln) oxides. However, the release of oxygen upon crystallization of pure lanthanide oxides is very small. It was figuratively classified as "smaller than the smallest".[26] So, oxygen dissolution in them is very small as well.

The dissolution of water vapor in pure alumina has been described.[30,31] However, no information is available on the dissolution of oxygen in pure alumina.[26] Though, as abovementioned, the oxygen presence in the medium influences both the composition of fused alumina and the peculiarities of melting and crystallization processes.[16,20] The deficiency or excess of oxygen is the most possible reason for the influence. Therefore, the first task of this work was the direct observation of gas release upon the crystallization of alumina melt and examination of the gas composition.

An increase in the specific volume upon the crystallization of Y_2O_3 and some alloys of the ZrO_2–Y_2O_3–Er_2O_3 system has been reported.[32,33] These results contradict those obtained by the levitation method.[10,15] The method for the estimation of volume change upon crystallization under the conditions of a center-symmetrical temperature field in the focal zone of an optical furnace has been proposed.[32–34] It has significant limitations and cannot be used for substances with high melt viscosity, disposed to the formation of internal hollow spaces, to which Al_2O_3 is related. Nevertheless, the second task was to thoroughly research the solidification process of alumina in the focal zone of an optical furnace, and comparing the peculiarities of the alumina crystallization with the crystallization processes in REE oxides under the same conditions, and to estimate the influence of their peculiarities on the reliability of the reported results.[32,33]

In addition, crystallization of alumina and REE oxides under the above-mentioned conditions and at different cooling rates is characterized by other peculiarities. The third task of the present work was to consider them as well.

2. Experimental procedure

Concentrated light heating of the optical furnace has some peculiarities.[35] They are: light energy is directed to one side of a sample; light flow has high density and normal distribution of the energy flow density in the focal zone; the volume and mass of samples are not large; rates of heating and cooling are very high and experiments could be made both in protective and in oxidizing media.

Melting and crystallization of Al_2O_3 and REE oxides were performed in an optical furnace with three xenon radiators.[32] The heating light flow of the optical furnace could be changed slowly, rapidly, or blocked with a curtain shutter. Initial samples were pressed from powder in tablets and had cylindrical shape with a diameter of 20 mm and a height of up to 10–15 mm. A sample was placed in the focal zone in air. Then the top of it was melted and crystallized in the air several times, and the melt pool of 5–8 mm depth was formed. At the same time, the sample was rotated with a speed of 60 rpm in order to symmetrize the temperature field. Crystallization processes were conducted using various cooling rates. In all case shrinkage hollows and vacuoles were formed inside the Al_2O_3 ingots. Some of the ingots were obtained under the special conditions, when "bubbles" were observed on the ingot surfaces. If the melt depth of alumina before the beginning of crystallization was significant (about 7–8 mm) and the cooling process was sufficiently slow, then the bubbles on the ingots surfaces were not formed. It is possible that thick solid crust is formed on the ingot surface and it lost any plasticity. In this case a lot of cracks were formed in the crust. The rejected from the melt gas released away and the shrink cone shape is not changes on the ingot surface. If alumina melt depth before the beginning of crystallization was not so significant (about 5–6 mm), solid crust on the ingot surface kept plasticity for some time and gas rejected from the melt inflated the bubble on the ingot surface before the cracks formed. Such bubble formation special conditions were selected experimentally.

The crystallization processes were recorded by a video camera fixed perpendicularly to the sample rotation axis. These experiments made it possible to estimate the yttria specific volume increasing upon crystallization using the ingot side views and approximation of radial ingot symmetry and thus to raise the accuracy of the volume change determination in comparison with the earlier described method[34] up to 5%.

The method of gas chromatography in a helium flow was used for gas composition analysis inside hollows and vacuoles of alumina ingots. As a rule, numerous cracks are formed in alumina ingots under cooling.[17–19] So, the exchange between the gases in the hollows and the environment is possible. In order to avoid escape of gas ejected from melt into hollows, some ingots were quenched in melt of beeswax just upon the surface solidification. The decomposition of wax complex organic molecules occurred at high temperature, yielding coke and pitches, which occluded all cracks and prevented gas loss. The products of thermal decomposition of organic molecules are known to be free of oxygen. Therefore, the presence of the latter in ingot hollows can only be evidence of its releasing during melt crystallization.

In order to determine the composition of the gas filling closed hollows, alumina ingots were put into a closed box connected to the gas system of the chromatograph. The box was equipped with a screw press for breaking the ingots at a room temperature. The ingot was fixed on four props. The box was blown through by He for 10–15 min. Then the ingot was broken with the screw press. The mixture of the gas from hollows and He was directed

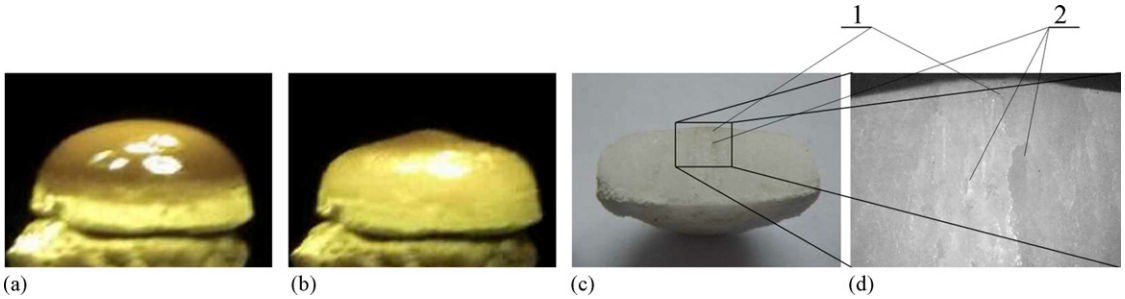

Fig. 1. Slow crystallization of Al_2O_3 ($U_{int} = 0.1$ mm/s): (a) initial melt pool; (b) ingot after crystallization; (c and d) ingot cross-section: (1) concentration regions of small pores and (2) shrinkage hollows.

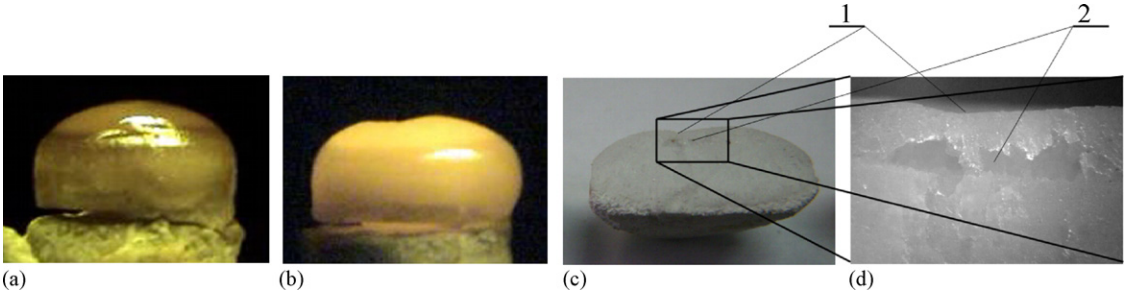

Fig. 2. Rapid crystallization of deep (6–7 mm) melt pool of Al_2O_3 ($U_{int} \approx 1$ mm/s): (a) initial melt pool; (b) ingot after crystallization; (c and d) ingot cross-section: (1) shrinkage cone and (2) shrinkage hollows.

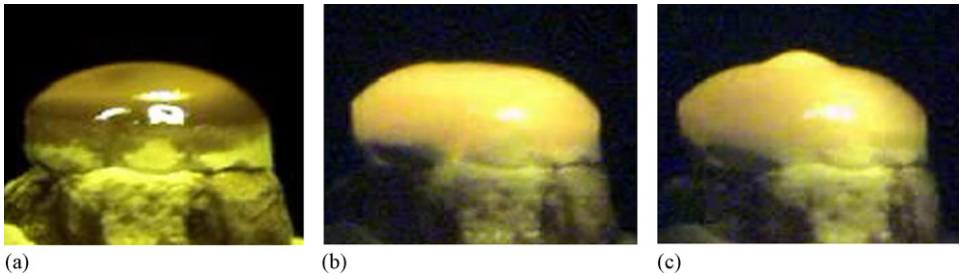

Fig. 3. More rapid crystallization of less deep (4–5 mm) Al_2O_3 pool melt, when the heating light flow was blocked with the curtain shutter ($U_{int} \geq 1$ mm/s): (a) initial melt pool; (b) the ingot 3 s after the light is blocked (shrinkage cone began to form); (c) ingot 4–5 s after the light is blocked, crystallization is complete and a bubble has formed on the ingot surface.

into the chromatograph. In such a way 10 ingots with surface bubbles were investigated. Five of them were obtained using air cooling and the others were quenched in the wax melt.

Also, the oxides of Y, Er, Ho, Tm, Yb, and Lu were crystallized under slow and rapid cooling in air.

According to the second task of this investigation, special attention was paid to the fabrication of yttria ingots under the described conditions and to estimation of their density by method of hydrostatic weighing in distilled water. In addition, yttria solid drops were smelted on a water-cooled substrate in the focal zone of the optical furnace. Their density was measured by the same method and the results were compared with the ones researches.[10,15]

3. Results

Depending on the rate of melt cooling, different processes of alumina ingot formation were observed. In all of the cases, shrinkage hollows were formed inside ingots due to a significant decrease of the specific volume during crystallization.

The sequences of shape changing of alumina melt pool surface at different crystallization rates is shown in Figs. 1–4. Three different processes accompanied the alumina crystallization in the described conditions:

- Gradual decrease in the heating light flow density provided slow decrease in the melt temperature, and the solid–melt interface moved from the edges and bottom to the surface center of the melt pool. The radial velocity of solid–melt interface of Al_2O_3 was $U_{int} = 0.1$ mm/s. The melt pool level was lowered, and salient cone formed in the ingot center (Fig. 1).
- Under rapid cooling ($U_{int} \approx 1$ mm/s), lowering of the melt pool level was insignificant, and a shrinkage cone formed in the ingot center (Fig. 2). The surface layer of the ingot was saturated with small pores.
- Under the most rapid cooling, when the light flow was blocked by the curtain shutter, a dense solid crust, plastic at high

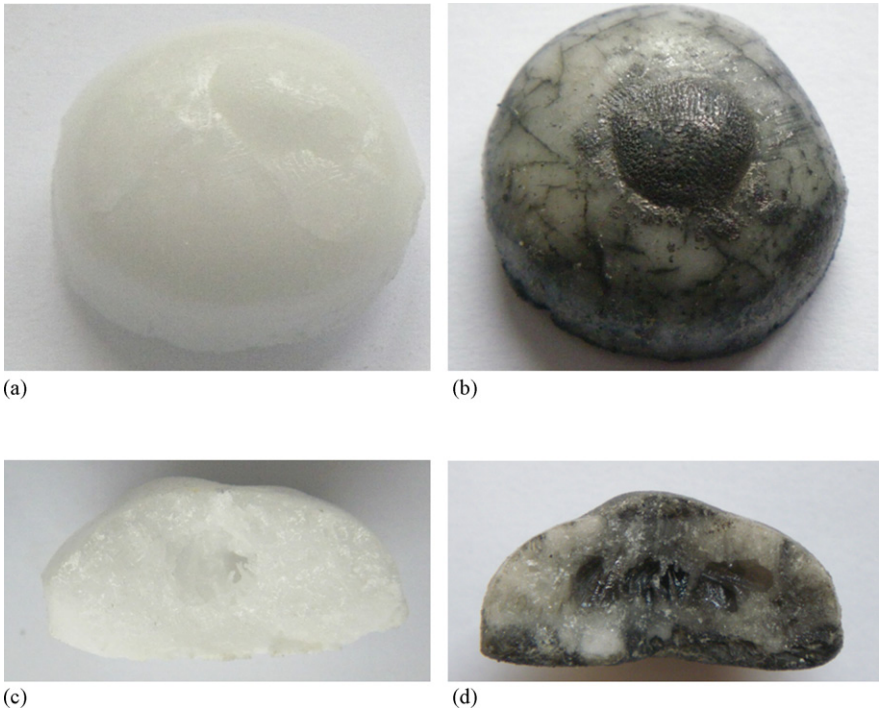

Fig. 4. The appearance of Al_2O_3 ingots (a and b) before and (c and d) after breakage. (a and c) Ingot obtained via cooling in air and (b and d) ingot obtained by quenching in wax melt.

temperature, immediately coated the ingot surface, and the crystallization proceeded from the surface, bottom and side edges of the melt pool to its volume center. In this case, crystallization conditions could be selected in such a way that at first a shrinkage cone began to form on the ingot surface, then in the area of the highest temperature the surface swelled up and a gas bubble formed in its center (Fig. 3). This phenomenon confirms that gas is ejected from the melt into the center of the melt volume when the Al_2O_3 lattice starts forming. In a deep melt pool, the solid surface crust had enough time to lose its plasticity and a surface bubble did not form.

The composition of the released gas during crystallization was investigated for the Al_2O_3 ingots obtained via rapid cooling. The appearance of the ingots is shown in Fig. 4.

Hollow spaces inside the ingots can be seen in Fig. 4(c) and (d). The cracks (Fig. 4b) and pores (Fig. 4d) were filled with coke and look like black streaks and top in the ingot quenched in the wax melt. The coke closed pores and cracks and thus the released oxygen did not leave hollows during cooling and washing with helium in the gas system of the chromatograph.

Among five Al_2O_3 ingots cooled in air and broken in the helium flow, oxygen was found in one ingot only, whereas the presence of oxygen in the gas system of the chromatograph was detected upon the breaking of all the ingots quenched in the wax melt. The volume of the opened hollows after the ingot breaking (V_{hol}) was determined using the method of hydrostatic weighing in distilled water.

The mean pressure of O_2 in ingot hollows $\bar{P}$ near the crystallization temperature (at $T_h \sim 2300$ K) and at the room temperature (at $T_r = 300$ K) was estimated using the Clapeyron–Mendeleev equation. $\bar{P} \approx 304$ kPa (3 atm) at $T = T_h \sim 2300$ K and $\bar{P} \approx 39.2$ kPa (0.39 atm) at $T = T_r = 300$ K.

The quantity of oxygen released from the quenched and broken ingots related to the ingot mass (M) was changing from 6×10^{-6} to 2×10^{-5} for different ingots. The mean ($\bar{M}$) was equal to:

$$\bar{M} = \frac{1}{5}\sum_{j=1}^{5}\left(\frac{M_{O_2\,j}}{m_{ing.j}}\right) \approx 8 \times 10^{-6} \quad (1)$$

where $M_{O_2\,j}$ is the oxygen mass released from hollows of j-th ingot and $m_{ing.j}$ is the mass of j-th ingot.

This estimation of the quantity and pressure of the oxygen released during alumina crystallization is rough because, firstly, the quantity of the oxygen released through the melt surface could not be calculated and, secondly, the cooling of the melted ingot was so rapid that the time between the surface solidification and the start of the ingot quenching was very short and inconstant. Therefore, an unknown part of the oxygen could escape to the environment through the cracks in the ingot surface before quenching. Thirdly, the estimation of the melted alumina mass was not exact because the fused part of the sample could not be completely separated from the unfused ceramic base. Moreover, some quantity of oxygen could be spent on the oxidation of wax organic molecules. For this reason special statistical methods for decreasing errors were not used.

It should be emphasize, that no other gaseous products were found in the gas released from broken alumina ingots at room temperature.

Like alumina, the oxides of Y, Er, Ho, Tm, Yb, and Lu were melted and crystallized with different cooling rates. All of three

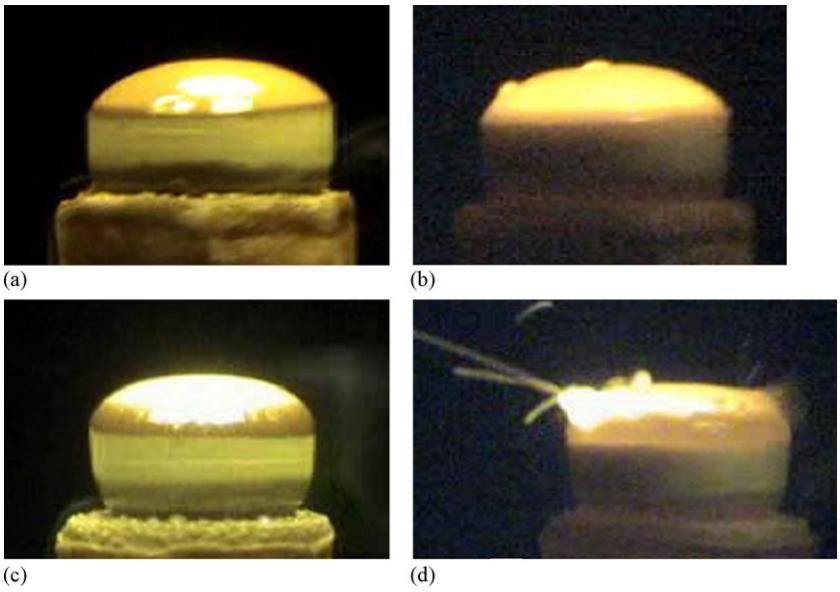

Fig. 5. Bubble formation on the ingot surfaces in the case of the most rapid crystallization: (a and c) melt pools of yttria and lutecia, respectively and (b and d) bubble formation on the surfaces of yttria and lutecia, respectively.

kinds of processes specific for the alumina crystallization were observed in the crystallization of yttria and the above-listed REE oxides. However, some differences were revealed, since each of their melts dissolved different quantity of oxygen and their viscosity was lower than that of alumina.

Under the most rapid cooling, bubble formation was observed for all oxides. Among the investigated oxides, the biggest gas release occurred in the crystallization of Lu, Ho, Yb, and Tm oxides. The gas ejection from Lu_2O_3 was so large that the melt splashing took place. The amount of gas released from erbia and yttria under the same conditions was lower than that from other oxides. Different moments of bubble formation on surface of yttria and lutecia are demonstrated in Fig. 5.

Like Al_2O_3 crystallization, decreased crystallization rate could lead to the formation of salient cones of solid phase saturated with gaseous pores in the ingot centers of the oxides. However, remelting destroyed the cones, and the solid ingot surfaces of erbia, thulia, and itterbia practically coincided with their initial melt surfaces. One can therefore concludes that the apparent specific volume of erbia, thullia, and itterbia do not change upon crystallization in the limits of the used method accuracy.

Upon slow lutecia crystallization the melt surface slightly lowered and the top of a porous salient cone took place, in such a way that the top of the cone became lower than the initial melt surface. This testified that the specific volume of lutecia diminished upon crystallization. In general, the results of the present investigation of the specific volume change in Y, Er, Ho, Tm, Yb and Lu oxides during crystallization differed from the results obtained using the levitation method.[15]

Special attention was paid to the investigation of yttria crystallization. The side views of melt pools and ingots of Y_2O_3 and Lu_2O_3 obtained via slow crystallization ($\tau \approx 100$ s) in the focal zone are shown in Fig. 6.

The apparent change of specific volume was estimated using the side views of the melt pool and ingot and axial symmetry approximation.

$$\frac{\Delta V}{V} = \frac{V_m - V_{sol}}{V_{sol}}$$

where V_m and V_{sol} are volumes of melt and solid phases, respectively.

$\Delta V/V$ of Y_2O_3 was found to equal ≈4%.

There were no shrinkage holes or hollows (bubbles) on the ingot cross-section.

In order to compare the present findings with the results obtained using the levitation method,[10,15] Y_2O_3 solid drops were smelted on a water-cooled copper substrate in the focal zone of the optical furnace. They were almost spherical with a diameter of 1.5–3 mm and had salient cones. Typical shapes of liquid and solid drops during and after crystallization process are shown in Fig. 7.

Porosity of the Y_2O_3 drops and samples cut out from the central zones of the Y_2O_3 ingots was measured using the method of hydrostatic weighing. The weighing accuracy was up to 0.0001 g and the weighing error did not exceed 0.5–1%. The results obtained showed that both kinds of samples did not have open porosity. The closed porosity was calculated at room temperature with comparison method of findings with the X-ray density of cubic Y_2O_3, $\rho_{Y_2O_3} = 5.0259$ (g/cm^3).[36] It was changing from 2% to 2.5% for both the solid drops and the samples cut out of the central part of ingots.

Thus, the following three kinds of processes accompany the crystallization of the Al, Y, Er, Ho, Tm, Yb, and Lu oxides in the center-symmetrical temperature field in oxygen mean and depend on the cooling rate:

- Ejection of the dissolved in the melt oxygen with the formation of surface bubbles and splashing of melted drops under rapid crystallization.

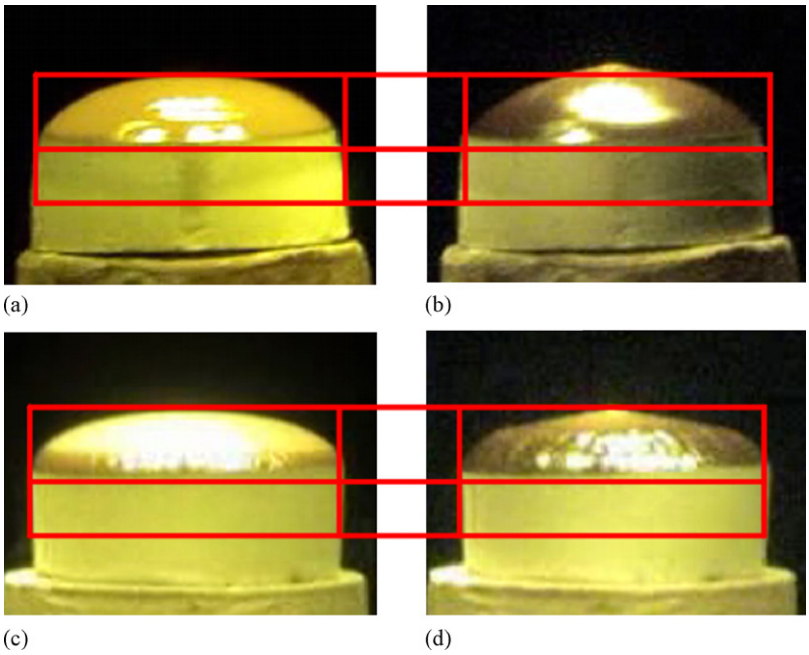

Fig. 6. The side views of (a) melt pool and (b) ingot of Y_2O_3 obtained upon slow crystallization ($\tau \approx 100$ s); (c and d) the same for Lu_2O_3.

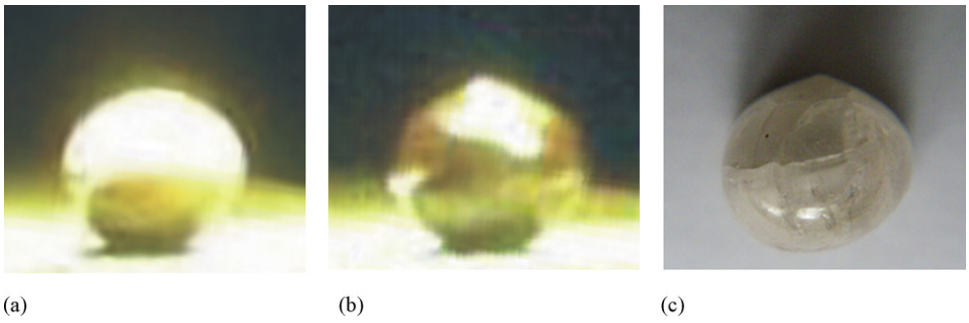

Fig. 7. Crystallization of an Y_2O_3 drop in the focal zone: (a) start of crystallization; (b) end of crystallization; (c) solid drop.

- Decrease of specific volume of Al_2O_3 and Lu_2O_3 and the absence of it (within limits of the experimental error) in Er_2O_3, Ho_2O_3, Tm_2O_3, and Yb_2O_3, or increase the specific volume of Y_2O_3, which is accompanied by a salient cone formation on the ingot surface under slow crystallization.
- Formation of a salient cone from a foam-like solid phase on the ingot surface under slow crystallization, which is accompanied by surface lowering. This is the most characteristic for Al_2O_3 and Lu_2O_3 and also occurs in other investigated oxides but in a less degree. Remelting decreases or destroys the foam-like volume of ingots.

4. Discussion

The main feature of this work is a direct observation of the ejection of dissolved oxygen from the melts of alumina, yttria and REE oxides of yttrium subgroup accompanied by gas bubbles formation and melt splashing during crystallization and estimation of the minimal quantity of oxygen dissolved in the alumina melt. In the case of melting in an oxidizing medium, quantity of oxygen dissolved in the alumina melt was not less than 8×10^{-6} g in the 1 g of alumina (1). According to the observed dynamics of crystallization process, it is approximately equal to that in the melts of yttria and REE oxides. We did not investigate the melting of alumina in non-oxidizing atmospheres or vacuum because of technical problems but our work showed clearly that oxygen dissolves in alumina during melting in oxidizing atmosphere (in air). Therefore, oxygen shell not been ejected from the melt into inside hollows or environment during crystallization Al_2O_3 melted in argon or vacuum. One conclusion of the reference[25] is "the use of non-oxidant atmospheres has been determinant in order to obtain crystals with no porosity. This fact can be explained if the gas dissolved in the melt is oxygen". Thus, our results had confirmed that the gas, dissolved in the alumina melt and rejected upon crystallization at the experimental conditions, is oxygen[25] (not air[23,24]).

Therefore, alumina is not an exception among the sesquioxides with a hexagonal structure: its melt dissolves approximately the same quantity of oxygen during melting in air.

An exact determination of the quantity of dissolved oxygen may be performed using a thermogravimetric analysis of alumina melting process, which accuracy or, in other words,

Table 1
The data on the melt density near the melting temperature and the volume effect of crystallization for Al_2O_3.

Reference	Density (g/cm^3)	$\Delta V/V$ (%)	Method for investigation	Medium
1	2.97	–	PD, SD	He
2	3.053	22	Arch	Ar
3	3.05	–	FD	Ar
4	2.7	20	SD	Vacuum
5	3.11	20	PQD	He
6	3.04	–	Arch	Ar, Vacuum
7	3.01	24	M	Vacuum
8	2.98	23.5	Arch	Ar, Vacuum
9	3.056	–	MPB	Ar, He
10	2.72	–	AL	Ar
11	3.06	–	MPB	90% Ar + 10% H_2
12	2.905	22.8	γ	Ar
13	2.79	–	AL	O_2, Ar, 95% Ar + 5% H_2
14	2.93	–	EL	Vacuum

Methods: Arch, Archimedes; FD, fall-drop; PQD, porosity of hardened drops; SD, sessile-drop; PD, pendant-drop; M, shape of meniscus in W and Mo ampoules; MPB, maximum pressure in a bubble; AL, aerodynamic levitation; EL, electrostatic levitation; γ, absorption of γ-quantum.

sensitivity of the balance must not be lower than 10^{-5} to 10^{-6} g at 2600–2700 K.

The significant specific volume decrease upon crystallization (by 20–24%) is another peculiarity of Al_2O_3 (Table 1).

It should be emphasized that the data on the alumina density at the melting temperature obtained by different researches are characterized by wide discrepancy (Table 1). They have been analyzed in some works.[9,11,12,14] One can easily see the difference the data obtained via gas levitation[10] and contact methods (when the solid–melt interfaces play role). It is up to 8–10% and may be caused by pollution with the container or capillary materials, for example MPB method, because pollution influences the alumina melting temperature, and the density at the melting or crystallization temperature changes correspondingly.[16] Nevertheless, such pollutions were absent in the pendant-drop method. Therefore another reason for these data discrepancy should be found.

The foregoing review and the obtained data confirm that the melting temperature of alumina decreases in the case of melting in an oxidizing medium. Hence the melt density must increase. The change in the melting temperature upon oxygen dissolution must also influence the melt density of the other investigated oxides in the same way. The existence of heterogeneous nucleation boundaries influences the crystallization temperature and the melt density at this temperature. Acoustic vibrations existed in the gas levitation method and other perturbing factors affect these parameters as well.[13,16] All this confirms once again that the peculiarities and errors of experimental methods should be taken into consideration in comparison of the physical properties data obtained by different methods.

The value of the alumina density at the melting temperature obtained with a gas levitation method, $d = 2.72$ (g/cm^3),[10] is lower than the mean values obtained with "contact" methods[1–3,5–9,11,12] on average by 8–10%. Therefore, one can expect that the data on the melt density at the crystallization temperature, for example, for yttrium and REE oxides obtained under the same conditions[15] are understated by 8–10% as well. Hence the crystallization volume effects calculated with these data are overstated. Moreover, the latest data on the alumina melt density at the crystallization temperature obtained by update levitation methods were 2.79 (g/cm^3)[13] and 2.93 (g/cm^3).[14] They are closer to the data of "contact" methods used in the present work. In addition, the values of crystallization volume effect were calculated on the basis of the data of melt density measured by a gas levitation method[10,15] and the X-ray density data for solids.[37] So they contain the above-considered possible errors of the gas levitation method, whereas the volume changes during crystallization observed directly in this work and before[30] have errors of the specific volume measurement connected with the presence of volume defects and incomplete separation of the fused ingot from the initial ceramic base.

It is worth noting a possibility of another mechanism of a salient cone formation. Large increase in the surface tension with decreasing temperature may cause diminution of the meniscus curvature radius of the melt pool, which leads to the center elevation above the rest of the ingot surface during crystallization. However, such processes must be accompanied with lowering the surface level around the ingot center, and the shape of the ingot surface must be like that of lutecia ingot (Fig. 6d). So, two mechanisms may take part in the formation of ingot surface of luttecia: convection movement of foam-like volume to the ingot center and large increasing of the surface tension with temperature decreasing.

However, direct observation of the yttria crystallization dynamics makes it possible to have preference for the model (mechanism) of specific volume increasing upon crystallization.

The direct observation method of the volume change used in this work should be related to contact methods because solid–liquid interface existed before the crystallization starts. So, it is characterized by existing errors in this method, which must be taken into account in comparison to the data obtained by itself and levitation methods. The use of this method with calculation of the porosity of obtained ingots and solid drops makes it possible to conclude that the specific volume of yttria increases during crystallization is no less than 1.5–2%.

5. Conclusion

Direct evidences of oxygen dissolution in alumina during melting in an oxidizing atmosphere (in air) and its ejection during crystallization are presented. The quantity of dissolved oxygen is not less than 8×10^{-6} g in the 1 g of alumina. The oxygen release upon the crystallization of alumina is comparative to that for REE oxides.

Increase in the Y_2O_3 specific volume during crystallization with taking into account the porosity of fused yttria has been confirmed. The specific volume of lutecia decreases, whereas that of the Er, Ho, Tm, and Yb oxides does not change, in a practical manner.

References

1. Kingery WD. Surface tension of some oxides and their temperature coefficients. *J Am Ceram Soc* 1959;**42**(1):6–10.
2. Kirshenbaum AD, Cahill JA. The density of liquid aluminum oxide. *J Inorg Nucl Chem* 1960;**14**:283–7.
3. Maurakh MA, Mitin BS, Roitberg MB. Contactless measurement of density and surface tension of liquid oxides at high temperature. *Zavodskaya Lab* 1967;**33**(8):984–5 [in Russian].
4. Zubarev YuV, Kostikov VI, Mitin BS, Nagibin YuA, Nishcheta VV. Some properties of liquid alumina. *Izv Akad Nauk SSSR Inorg Mater* 1969;**5**(9):1563–5 [in Russian].
5. Tyrolerova P, Lu W-K. Volume change on freezing of Al_2O_3. *J Am Ceram Soc* 1969;**52**(2):77–9.
6. Mitin BS, Nagibin YuA. Density of liquid alumina. *Russ J Phys Chem* 1970;**44**:1325–6 [in Russian].
7. Rasmussen JJ, Nelson RP. Surface tension and density of molten Al_2O_3. *J Am Ceram Soc* 1971;**54**(8):398–401.
8. Elyutin AD, Mitin BS, Nagibin YuA. Properties of liquid alumina. *Izv Akad Nauk SSSR Inorg Mater* 1972;**8**:477–80 [in Russian].
9. Shpil'rain EE, Yakimovich RA, Tsitsarkin AF. Experimental study of density of liquid alumina up to 2750 °C. *High Temp High Press* 1973;**5**:191–8.
10. Granier B, Heurtault S. Méthode mesure de la densité de réfractaires liquids. Application á l'alumine et á l'oxyde d'yttrium. *Rev Int Hautes Tempér Réfract Fr* 1983;**20**:61–7.
11. Ikemiya N, Umemoto J, Hara S, Ogino K. Surface tensions and densities of molten Al_2O_3, Ti_2O_3, V_2O_5 and Nb_2O_5. *ISIJ Int* 1993;**33**(1):156–65.
12. Stankus SV, Tyagelsky PV. Thermal properties of Al_2O_3 in the melting region. *Int J Thermophys* 1994;**15**(2):309–16.
13. Glorieux B, Millot F, Rifflet J-C, Coutures J-P. Density of superheated and undercooled liquid alumina by a contactless method. *Int J Thermophys* 1999;**20**(4):1085–94.
14. Paradis P-F, Ishikawa T, Saita Yu, Yoda S. Non-contact thermophysical property measurements of liquid and undercooled alumina. *Jpn J Appl Phys* 2004;**43**:1496–500.
15. Granier B, Heurtault S. Density of rare-earth sesquioxides. *J Am Ceram Soc* 1988;**71**(11):C-466–8.
16. Schneider SJ, McDaniel CL. Effect of environment upon the melting point of Al_2O_3. *J Res Natl Bur Stand A: Phys Chem* 1967;**71A**(4): 317–33.
17. Nelson LS, Richardson NL, Keil K, Skaggs SR. Effects of oxygen and argon atmospheres on pendant drops of aluminum oxide melted with carbon dioxide laser radiation. *High Temp Sci* 1973;(5):138–54.
18. Coutures J-P, Rifflet J-Cl, Florian P, Massiot D. Etude par analyse thermique et par RMN très haute température de ^{27}Al de la solidification de Al_2O_3 en l'absence de nucleation hétérogène: effets de la temperature du liquide et de la pression partielle d'oxygène. *Rev Int Hautes Tempér Réfract Fr* 1994;**29**:123–42.
19. Weber KR, Anderson CD, Merkley DR, Nordine PC. Solidification behavior of undercooled liquid aluminum oxide. *J Am Ceram Soc* 1995;**78**(3):577–82.
20. Vorob'ev AYu, Petrov VA, Titov VE, Ulybin SA. The effect of vacuum on the reflectivity of alumina ceramics under conditions of melting by concentrated laser radiation and subsequent free cooling. *High Temp* 2007;**45**(6):779–84.
21. Glorieux B, Millot F, Rifflet JC. Surface tension of liquid alumina from contactless techniques. *Int J Thermophys* 2002;**23**(5):1249–57.
22. Coutures GP, Foëx M, Chaurdon MG. Influence de la pression d'oxygène sur la temperature de solidification de certains oxides des elements de transition. *C R Acad Sci Paris Series C* 1968;**267**:C-1577–80.
23. Saito M. Gas bubble formation of ruby single crystals by floating zone method with an infrared radiation convergence type heater. *J Cryst Growth* 1985;**71**:664–72.
24. Saito M. Growth process of gas bubble in ruby single crystals by floating zone method. *J Cryst Growth* 1986;**74**:385–90.
25. Oliete PB, Pena JE. Study of the gas inclusion in $Al_2O_3/Y_3Al_5O_{12}$ and $Al_2O_3/Y_3Al_5O_{12}/ZrO_2$ eutectic fibers grown by laser floating zone. *J Cryst Growth* 2007;**304**:514–9.
26. Coutures J-P, Verges R, Foëx M. Valerus comparées des temperatures de solidification des différents sesquioxydes de terres rares; influence de l'atmosphère. *Rev Int Hautes Tempér Réfract Fr* 1975;**12**(2):181–5.
27. Coutures J-P. Contribution a l'étude du comportement de I'oxyde cobalteux liquide en atmosphère oxydante. *Rev Int Hautes Tempér Réfract Fr* 1973;**10**(1):39–57.
28. Coutures J-P, Berjoan R, Granier B. Utilisation des fours solaires pour l'étude des interactions gaz oxides liquids. *Rev Int Hautes Tempér Réfract Fr* 1973;**10**(4):273–81.
29. Coutures J-P. Interactions gaz-oxydes liquids purs ou complexes: aspects fondamentaux et appliqués. *Rev Int Hautes Tempér Réfract Fr* 1979;**16**:211–24.
30. Diamond JJ, Drago AJ. Studies of molten alumina in the arc-image furnace. *Rev Int Hautes Tempér Réfract Fr* 1966;**3**(3):273–9.
31. Coutures J-P, Devauchelle JM, Munoz R, Urbain G. Dissolution of water vapor in SiO_2–Al_2O_3 melts. *Rev Int Hautes Tempér Réfract Fr* 1980;**17**:351–61.
32. Frolov AA, Anrievskaya ER, Kornienko OA, Frolov YuA. Specifics of crystallization of highly refractory alloys based on zirconium, yttrium, and erbium oxides. *Refract Ind Ceram* 2007;**48**(3):185–8.
33. Frolov A, Frolov Y, Andrievskaya E. Anomalous crystallization of some alloys in refractory oxide systems based on zirconia, yttria and erbia. *High Temp Mater Processes* 2007;**26**(3):221–9.
34. Frolov AA, Voinich EV, Frolov YuA. Method for evaluating the change in specific volume of refratory substances during crystallization. *Refract Ind Ceram* 2008;**49**(3):183–8.
35. Laslo TS. Image furnace techniques. *Technique of inorganic chemistry*, vol. 5. New York: Interscience Publishers; 1965.
36. Antic B, Mitric M, Rodic D. Structure properties and magnetic susceptibility of diluted magnetic semiconductor $Y_{2-x}Ho_xO_3$. *J Magn Magn Mat* 1995;**145**:349–56.
37. Foex M, Traverse JP. Remarques sur les transformations critallines présentées a hounte temrérature par les sesquioxyses de terres rares. *Rev Int Hautes Tempér Réfract* 1966;**3**:429–53. Diffraction data card file ASTM 1990 №. 20-1412.